J Neurophysiol 113: 1358–1368, 2015.
First published December 4, 2014; doi:10.1152/jn.00573.2014.

Synaptic mechanisms for generating temporal diversity of auditory representation in the dorsal cochlear nucleus

Mu Zhou,[1,4] Ya-Tang Li,[1,4] Wei Yuan,[1,5] Huizhong W. Tao,[1,3] and Li I. Zhang[1,2]

[1]*Zilkha Neurogenetic Institute, Keck School of Medicine, University of Southern California, Los Angeles, California;* [2]*Department of Physiology and Biophysics, University of Southern California, Los Angeles, California;* [3]*Department of Cell and Neurobiology, University of Southern California, Los Angeles, California;* [4]*Graduate Programs, University of Southern California, Los Angeles, California; and* [5]*Department of Otolaryngology of Southwest Hospital, Third Military Medical University, Chongqing, China*

Submitted 4 August 2014; accepted in final form 1 December 2014

Zhou M, Li YT, Yuan W, Tao HW, Zhang LI. Synaptic mechanisms for generating temporal diversity of auditory representation in the dorsal cochlear nucleus. *J Neurophysiol* 113: 1358–1368, 2015. First published December 4, 2014; doi:10.1152/jn.00573.2014.—In central auditory pathways, neurons exhibit a great diversity of temporal discharge patterns, which may contribute to the parallel processing of auditory signals. How such response diversity emerges in the central auditory circuits remains unclear. Here, we investigated whether synaptic mechanisms can contribute to the generation of the temporal response diversity at the first stage along the central auditory neuraxis. By in vivo whole-cell voltage-clamp recording in the dorsal cochlear nucleus of rats, we revealed excitatory and inhibitory synaptic inputs underlying three different firing patterns of fusiform/pyramidal neurons in response to auditory stimuli: "primary-like," "pauser," and "buildup" patterns. We found that primary-like neurons received strong, fast-rising excitation, whereas pauser and buildup neurons received accumulating excitation with a relatively weak fast-rising phase, followed by a slow-rising phase. Pauser neurons received stronger fast-rising excitation than buildup cells. On the other hand, inhibitory inputs to the three types of cells exhibited similar temporal patterns, all with a strong fast-rising phase. Dynamic-clamp recordings demonstrated that the differential temporal patterns of excitation could primarily account for the different discharge patterns. In addition, discharge pattern in a single neuron varied in a stimulus-dependent manner, which could be attributed to the modulation of excitation/inhibition balance by different stimuli. Further examination of excitatory inputs to vertical/tuberculoventral and cartwheel cells suggested that fast-rising and accumulating excitation might be conveyed by auditory nerve and parallel fibers, respectively. A differential summation of excitatory inputs from the two sources may thus contribute to the generation of response diversity.

central auditory pathway; in vivo whole-cell recording; voltage clamp; synaptic input; excitatory/inhibitory balance

ALTHOUGH AUDITORY NERVE FIBERS exhibit more or less uniform temporal discharge patterns in response to a certain sound stimulus (Kiang et al. 1965), a diversity of discharge patterns is observed for neurons at almost every processing stage along the central auditory pathway. For example, in response to tone stimulation, although a population of neurons does inherit the primary-like discharge pattern from the auditory nerve, many other neurons in the dorsal cochlear nucleus (DCN) (Godfrey et al. 1975; Hancock and Voigt 2002; Rhode and Kettner 1987; Rhode and Smith 1986), inferior colliculus (Ehret and Merzenich 1988; Kuwada et al. 1997; Semple and Kitzes 1985), and even auditory cortex (Recanzone 2000) exhibit "pauser" and "buildup" response patterns, which are distinct from auditory nerve responses. These diversified discharge patterns may be relevant for the representation and processing of specific sound-information components. However, how such functional diversity is created at the first central station along the afferent auditory pathway remains unclear.

One recent model proposes that variations in the availability of an intrinsic, rapidly inactivating A-type K^+ conductance and its activation status can result in a variation in the first spike latency and first interspike interval, as observed for different discharge patterns (Kanold and Manis 1999, 2005; Manis 1990). Other studies suggest that diverse response types of fusiform cells may result from the heterogeneity in their specific synaptic circuitry (Godfrey et al. 1975; Hancock and Voigt 2002; Kuwada et al. 1997). However, what synaptic mechanisms could contribute to the generation of response diversity remains unknown.

Synaptic connections in the DCN have been studied mostly in in vitro preparations. It is generally thought that pyramidal neurons receive direct auditory nerve inputs on their basal dendrites in the deep layer (Brown and Ledwith 1990; Ryugo and May 1993), as well as auditory and nonauditory inputs on their apical dendrites in the superficial layer (Mugnaini et al. 1980; Oertel and Young 2004). The pyramidal neurons also receive inhibitory inputs from various sources, including cartwheel cells in the superficial layer, vertical/tuberculoventral cells in the deep layer, and possibly the D-multipolar cells in the posterior ventral part of the cochlear nucleus (Golding and Oertel 1997; Kuo et al. 2012; Nelken and Young 1994; Oertel and Young 2004). It is possible that this rich repertoire of synaptic inputs can result in summed excitation and inhibition with diverse temporal patterns. In this study, we performed sequential loose-patch/current-clamp and voltage-clamp recordings from the same DCN pyramidal neurons in vivo. This allowed us to correlate directly the spike response pattern of the cell with the temporal patterns of underlying excitatory and inhibitory synaptic inputs and to determine how the excitatory and inhibitory interplay shapes the output spike response. Our results revealed that the response diversity of DCN pyramidal neurons could be largely explained by the

Address for reprint requests and other correspondence: L. I. Zhang, Dept. of Physiology and Biophysics, Univ. of Southern California, 1501 San Pablo St., Rm. 431, Los Angeles, CA 90033 (e-mail: liizhang@usc.edu).

differential temporal patterns of synaptic inputs that they received under our experimental conditions.

MATERIALS AND METHODS

All experimental procedures used in this study were approved under the Animal Care and Use Committee at the University of Southern California (Protocol Number: 11759).

Animal preparation. Experiments were performed on 101 female Sprague-Dawley rats (~3 mo old, weighing 250–300 g, raised with a 12-h light/dark cycle). Rats were anesthetized with ketamine (60 mg/kg ip) and xylazine (8 mg/kg ip). During the experiments, the level of anesthesia was monitored by checking the animal's responses to toe pinch. Ketamine, at one-third of the initial dosage, was administered every ~45 min. The body temperature was maintained at 37.5°C by a feedback heating system (Harvard Apparatus, Holliston, MA). The animal was positioned with the left ear facing a calibrated free-field speaker (Vifa, Copenhagen, Denmark) in a sound-attenuation booth (Acoustic Systems, Houston, TX). A sound-attenuating plug was inserted into its right ear. After opening the left part of the occipital bone, part of the cerebellum was aspirated to expose the left DCN. During the experiment, DCN was covered with an artificial cerebrospinal fluid (ACSF; in mM: 124 NaCl, 1.2 NaH_2PO_4, 2.5 KCl, 25 $NaHCO_3$, 20 glucose, 2 $CaCl_2$, 1 $MgCl_2$). We mapped the DCN tonotopy with extracellular recordings, which demonstrated a low-high frequency gradient along the lateral-medial axis, as described in our previous study (Zhou et al. 2012).

In vivo whole-cell and loose-patch recordings. Whole-cell recordings were made with an Axopatch 200B amplifier (Molecular Devices, Sunnyvale, CA). Patch pipettes made from borosilicate glass capillaries (Kimax) had an impedance of 4–5 MΩ. Pipettes contained a potassium-based solution (in mM): 130 K-gluconate, 4 MgATP, 0.3 GTP, 8 phosphocreatine, 10 HEPES, 11 EGTA, 5 KCl, 1 $CaCl_2$, 0.25 fluorescein dextran, pH 7.3. The patch pipette was lowered into the DCN at an angle of ~85°. The brain stem surface was covered with 3.5% agar, prepared in warm ACSF. Whole-cell capacitance was fully compensated, and the initial series resistance (25–50 MΩ) was compensated for 40–60% to achieve an effective series resistance of 15–30 MΩ. Signals were filtered at 5 kHz and sampled at 10 kHz. Only cells with their resting membrane potential, more hyperpolarized than −50 mV, were studied. Pyramidal neurons were recorded at 100- to 250-μm depths below the surface, corresponding to the pyramidal cell layer (Mugnaini et al. 1980; Wouterlood and Mugnaini 1984). The reconstructed morphologies of some recorded neurons confirmed the pyramidal neuron type [see our previous study (Zhou et al. 2012)].

Two major types of inhibitory neurons were also recorded in this study. Vertical cells were recorded at 250- to 700-μm depths (Mugnaini et al. 1980; Rhode 1999) and identified by their lack of spontaneous activity and absence of responses to broad-band noise stimulation (Rhode 1999; Spirou et al. 1999; Young and Brownell 1976). Cartwheel cells were recorded at 80- to 150-μm depths (Wouterlood and Mugnaini 1984) and identified by the firing of complex spikes (Manis et al. 1994; Parham and Kim 1995; Portfors and Roberts 2007). Loose-patch, cell-attached recordings were performed with pipettes of smaller tip openings (impedance ~10 MΩ) so as to overcome the recording bias toward larger cells (Wu et al. 2008). Pipettes were filled with ACSF. Loose seal (100–200 MΩ) was made from the neuron, allowing spikes only from the patched cell to be recorded. Recording was made under voltage clamp. Signals were filtered at 0.3–10 kHz.

Sound stimulation. Software for sound stimulation and data acquisition was custom developed with LabVIEW (National Instruments, Austin, TX). For each successful whole-cell recording, we first mapped the tonal receptive field (TRF) for the recorded cell under current clamp. Pure tones (0.5–64 kHz at 0.1 octave intervals, 50 ms duration, 3 ms ramp) at eight, 10 dB-spaced sound intensities [0–70 dB sound-pressure level (SPL)] were delivered pseudorandomly. The time interval and intensity difference between two sequential tones were set at 0.5–1 s and no more than 30 dB SPL, respectively, to ensure minimal cross-interactions between the stimuli. Characteristic frequency (CF), the frequency at which the neuron responded to tones with minimum intensity, was determined online. Then, the responses of the same cell to 10 repetitions of CF tone stimulation at 60 dB SPL were recorded with the cell clamped at −70 and 0 mV, respectively. An interstimulus interval of 4.5 s was used to minimize cross-trial interactions. After this, the cell's responses to 40 repetitions of 60 dB SPL CF tone stimulation were recorded under current clamp. Four different durations were presented: 25, 50, 100, and 200 ms. The same sound-stimulation protocol was applied for loose-patch recordings.

Data analysis. Spikes from either current-clamp recordings or loose-patch recordings were sorted offline. The neuronal response type was determined based on the peristimulus spike time histogram (PSTH) in response to 60 dB SPL CF tone stimulation. The first spike latency was determined by the time point in the PSTH, where firing rate exceeded the average spontaneous firing rate by 3 SD of baseline activity. Evoked firing rate was calculated by subtracting the spontaneous rate firing from the firing rate within a defined time window. All of the synaptic response traces evoked by the same test stimulus were averaged. Onset latency was determined by the time point where the current amplitude exceeded the average baseline by 3 SD. In current-clamp recordings, subthreshold membrane-potential responses were obtained by removing spikes with a 3-ms median filter [each data point was replaced by the median of data points within a time window ±1.5 ms of this data point; see Chung and Ferster (1998) and Jagadeesh et al. (1997)].

Excitatory and inhibitory synaptic conductances were derived (Sun et al. 2010; Wu et al. 2008; Zhang et al. 2003, 2011), according to $\Delta I = G_e \cdot (V - E_e) + G_i \cdot (V - E_i)$. ΔI is the amplitude of the synaptic current response at any time point after subtraction of the baseline current; G_e and G_i are the excitatory and inhibitory synaptic conductance, respectively; V is the holding voltage; and E_e (0 mV) and E_i (−70 mV) are the excitatory and inhibitory reversal potentials, respectively. The clamping voltage V was corrected from the applied holding voltage (V_h): $V = V_h - R_s \cdot I$, where R_s is the effective series resistance. An estimated junction potential of −11 mV was corrected. By holding the recorded cell at two different voltages (the reversal potentials for excitatory and inhibitory current, respectively), G_e and G_i could be resolved from the equation.

The expected membrane-potential change caused by synaptic conductances was derived with an integrate-and-fire neuron model (Liu et al. 2007; Somers et al. 1995): $V_m\,(t + dt) = -dt/C\{G_e(t)\cdot[V_m(t) - E_e] + G_i(t)\cdot[V_m(t) - E_i] + G_r\,[V_m(t) - E_r]\} + V_m(t)$, where $V_m(t)$ is the membrane potential at time t; C is the whole-cell capacitance; G_r is the resting leaky conductance; and E_r is the resting membrane potential (−60 mV). To simulate the spike response, 20 mV above the resting membrane potential was set as the spike threshold, and a 5-ms refractory period was used. C (20–50 pF) was measured during the experiment, and G_r was calculated based on the equation $G_r = C \cdot G_m / C_m$, where G_m, the specific membrane conductance, is 2e–5 S/cm^2, and C_m, the specific membrane capacitance, is 1e–6 F/cm^2 (Hines 1993; Stuart and Spruston 1998).

Fitting synaptic currents. Each phase of the synaptic current was fitted with an exponential function using MATLAB (MathWorks, Natick, MA). The equations to fit the two phases of the accumulating excitation (see Fig. 3*A*) were: $f(t) = 1 - \exp[-(t - t_1)/\tau_1]$ and $f(t) = k \cdot \{1 - \exp[-(t - t_2)/\tau_2]\} + \{1 - \exp[-(t_2 - t_1)/\tau_1]\}$, where t_1 and t_2 are onsets of each phase, and τ_1 and τ_2 are time constants. The equations to fit the fast-rising excitation and inhibition (see Fig. 3*A*) were: $f(t) = 1 - \exp[-(t - t_1)/\tau_1]$ and $f(t) = \exp[-(t - t_2)/\tau_2] \cdot \{1 - \exp[-(t_2 - t_1)/\tau_1]\}$.

Dynamic clamp. Dynamic-clamp recordings were carried out according to our previous studies (Li et al. 2012; Liu et al. 2011). The current injected to the cell was calculated in real time according to: $I(t) = G_e(t)\cdot[V_m(t) - E_e] + G_i(t)\cdot[V_m(t) - E_i]$.

The time-dependent G_e and G_i were simulated synaptic conductances. E_e and E_i (reversal potentials) were set as 0 mV and −70 mV, respectively. The membrane potential V_m (*t*) was sampled at 5 kHz.

Statistics. Shapiro-Wilk test was first applied to examine whether samples had a normal distribution. In the case of a normal distribution, *t*-test or one-way ANOVA with a post hoc Tukey test was applied. Otherwise, a nonparametric test was applied. Data were presented as mean ± SE if not specified otherwise.

RESULTS

Temporal response patterns of rat DCN pyramidal neurons. In the rat DCN, we first characterized the discharge patterns of pyramidal neurons located in *layer 2* (see MATERIALS AND METHODS). Cell-attached recordings (Wu et al. 2008, Zhou et al. 2012) were performed to record spikes from individual pyramidal neurons in the middle-frequency region (11.8 ± 3.7 kHz, mean ± SD). When the cells were tested with CF tones, buildup (30%), pauser (35%), and primary-like (35%) response patterns were widely observed (Fig. 1, *A* and *B*), consistent with previous studies (Hancock and Voigt 2002; Rhode and Smith 1986). As shown by the PSTH (Fig. 1, *A* and *B*), the primary-like discharge pattern started with a fast increase in firing, followed by sustained firing in the remaining duration of the tone (Fig. 1*B*). This discharge pattern in the rat DCN may correspond to the previously reported chopper pattern in other species, although for the latter, interspike intervals are much more uniform, resulting in regularly spaced peaks in the PSTH (Hancock and Voigt 2002; Rhode and Smith 1986). The pauser-discharge pattern started with a sharp, transient-onset response, which was followed by an ~15-ms period of silence and then an increase in firing to a level sustained in the remaining tone duration (Fig. 1*B*). The buildup pattern exhibited an initial silent period of ~15 ms, after which, the first spike appeared, and the firing rate was then increased gradually (Fig. 1*B*). Transient-onset responses were also observed in two cells (data not shown).

The most prominent difference among the three response patterns was for spikes occurring within the first 25-ms window after the stimulus onset. The buildup response exhibited a much longer first spike latency (19.8 ± 5.6 ms, mean ± SD) than the primary-like (5.2 ± 1.3 ms) and pauser responses (5.4 ± 0.8 ms; Fig. 1*C*). The primary-like response exhibited a significantly higher firing rate during the first 25-ms window (Fig. 1*D*) and a shorter interspike interval between the first and second spikes (i.e., the first interspike interval) compared with the pauser and buildup responses (Fig. 1*E*). As shown by the plot of evoked firing rate within the 4- to 9-ms time window after the tone onset (which contains the first evoked spike in primary-like and pauser patterns) against that within the 9- to 14-ms window after the tone onset (which contains the silent period in pauser and buildup patterns), the cells were segregated into three distinct clusters (Fig. 1*F*), demonstrating that different discharge patterns are clearly distinguishable. The spontaneous firing rate, on the other hand, was not different among the three types of cells (primary-like: 21.8 ± 3.2 Hz; pauser: 26.8 ± 4.1 Hz; buildup: 18.5 ± 4.3 Hz; one-way ANOVA, $F = 1.22$, $P = 0.30$).

Excitatory and inhibitory synaptic inputs to DCN pyramidal neurons. We next carried out whole-cell recordings to reveal the synaptic inputs underlying different discharge patterns. The discharge pattern of the recorded cell was first examined under current clamp, by applying repeated CF tones at 60 dB SPL (Fig. 2, *A* and *B*). Primary-like, pauser, and buildup spike patterns were all observed in the recorded cell population, similar to cell-attached recordings (Fig. 2*B*). Notably, they were associated with different subthreshold membrane-potential response patterns after filtering out the action potentials (Fig. 2*C*). The primary-like response was marked by a fast and strong depolarization, which was largely sustained during tone stimulation. The pauser response exhibited a sharp transient onset depolarization, followed by a brief hyperpolarization of ~10-ms duration, after which, the membrane potential gradually depolarized. The buildup response lacked a clear onset depolarization, and the membrane potential slowly depolarized from an early, brief hyperpolarization, which started at ~5 ms after the tone onset and lasted for ~10 ms.

Subsequently, we recorded excitatory and inhibitory currents under voltage clamp by clamping the cell's membrane potential at −70 and 0 mV, respectively (Fig. 2, *D* and *E*). Excitatory and inhibitory conductances were derived from the recorded currents (Fig. 2*F*; see MATERIALS AND METHODS). Whereas the inhibitory inputs to the three types of cells exhibited similar temporal profiles, the excitatory inputs were strikingly different (Fig. 2*F*). The primary-like cell exhibited "fast-rising" excitation, which rose rapidly to the peak before slowly decaying to a sustained level. In contrast, the pauser and buildup cells exhibited "accumulating" excitation: the excitation rose gradually without decaying. Furthermore, the pauser and buildup cells appeared to be distinguishable by the strength of the onset excitation.

We next examined whether the observed synaptic inputs can sufficiently account for the corresponding spike patterns of the recorded cells. With a single-compartment, integrate-and-fire neuron model, we derived the expected membrane potential and spike responses from the experimentally determined excitatory and inhibitory synaptic conductances (see MATERIALS AND METHODS). As shown for the three example cells, both the derived membrane potential (Fig. 2*G*) and spike (Fig. 2*H*) response patterns qualitatively matched the recorded membrane-potential and spike response patterns, respectively, suggesting that the temporal interplay of sound-evoked synaptic inputs may sufficiently result in distinct spike patterns.

Diversity in temporal dynamics of excitation. To quantify the temporal properties of synaptic responses, we performed curve fitting to the conductance traces using exponential functions (see MATERIALS AND METHODS). The accumulating excitation exhibited two rising phases (I and II) of different time constants, with *phase I* being fast and *phase II* being slow, whereas the fast-rising excitation, as well as the inhibition, exhibited only a single fast-rising phase (Fig. 3*A*). We quantified the amplitude of excitation or inhibition in each rising phase. Primary-like, pauser, and buildup cells were substantially different in the amplitude of *phase I* excitation, whereas they were not different in the amplitude of inhibition (Fig. 3*B*). Consequently, the excitation/inhibition (E/I) ratio between *phase I* excitation and inhibition was different among the three types of cells (Fig. 3*C*). The amplitude of *phase I* excitation, as

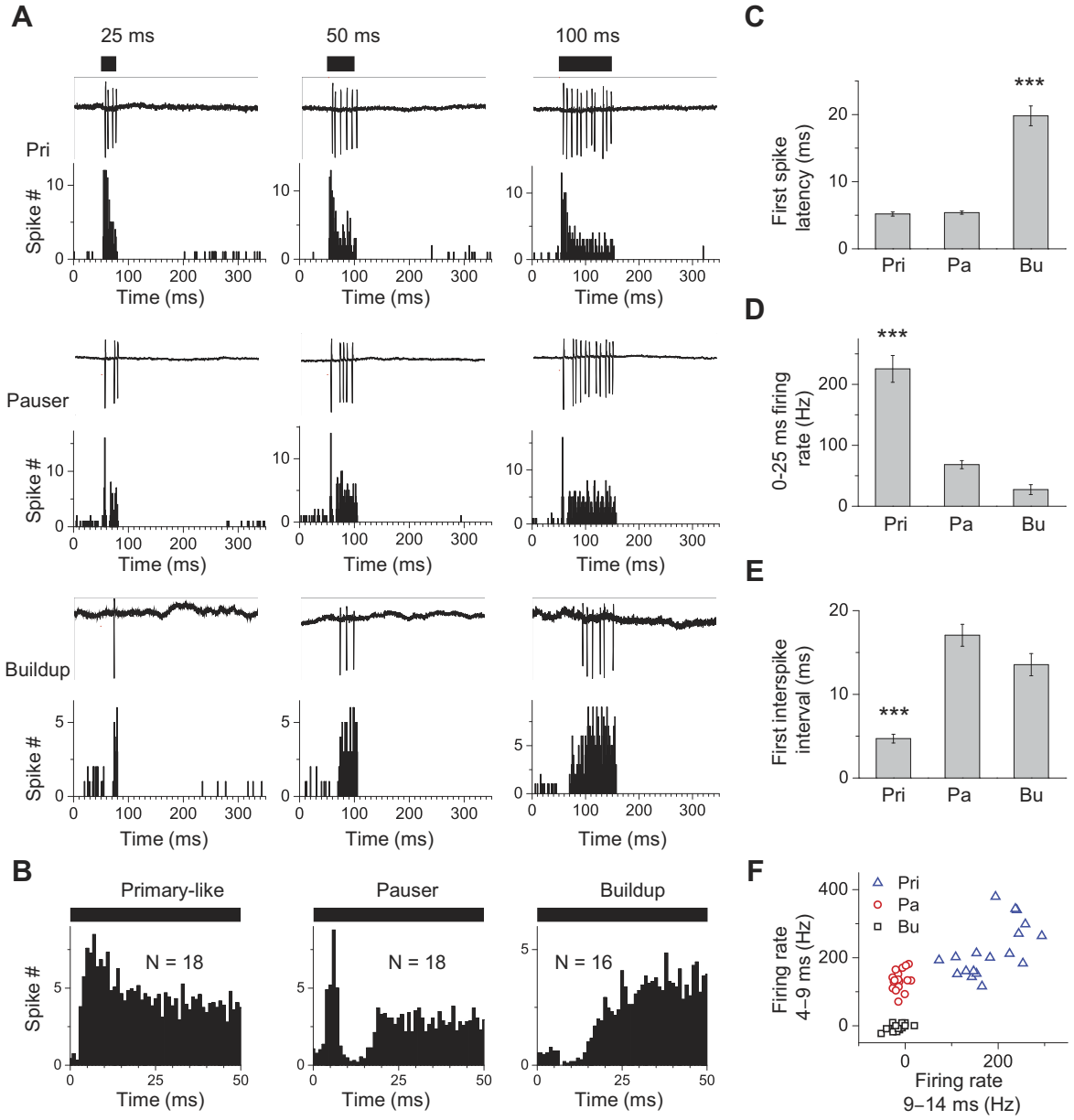

Fig. 1. Response diversity in the rat dorsal cochlear nucleus (DCN). *A*: spike patterns of 3 example pyramidal cells in response to characteristic frequency (CF) tones of different durations (marked by thick bars). For each cell, (*top*) sample recorded traces (in 1 trial) are shown, and (*bottom*) peristimulus spike time histograms (PSTHs; bin size = 1 ms) for responses in all trials are shown. *B*: average PSTHs (bin size = 3 ms) for all of the recorded cells of 3 response types. Cell numbers are marked. *C*: average spike latency for the 3 groups of cells. Bars = SE; ***$P < 0.001$, 1-way ANOVA and post hoc Tukey test (same as below). *D*: average firing rate within the 0- to 25-ms window after the tone onset. *E*: average interspike interval between the 1st and 2nd spikes. Note that the 1st interspike interval was relatively long in buildup cells, due to their low firing rates at the onset of tones. This is different from pauser cells, in which responses were suppressed after the 1st spike. *C–E*: cell numbers are the same as in *B*. *F*: plot of evoked firing rate (after subtraction of spontaneous firing) within the 4- to 9-ms window after the tone onset vs. that within the 9- to 14-ms window for all of the cells. Note that the precategorized, primary-like (Pri), pauser (Pa), and buildup (Bu) cell groups are well segregated.

well as the E/I ratio, was largest in primary-like cells and smallest in buildup cells (Fig. 3, *B* and *C*). On the other hand, the timing of the peak *phase I* excitation was not different among the three types of cells (Fig. 3*D*). As for *phase II* excitation, pauser and buildup cells had a similar amplitude, whereas the excitation in primary-like cells did not have a second rising phase (Fig. 3*E*). Furthermore, we did not find a difference in the onset latency of either excitation or inhibition among the three types of cells (Fig. 3*F*). Excitation always preceded inhibition by ~1.5 ms (Fig. 3*F*), suggesting a universal, disynaptic nature of the inhibitory input relative to the most rapid excitatory component.

We also measured the resting membrane potential in the absence of sound stimulation and the average potential within a 10-ms window right before the onset of sound-evoked responses, which occurred at ~4 ms (Fig. 3*F*) after the stimulus onset (i.e., a window that covers ~6 ms before and ~4 ms after the onset of sound). There were no obvious hyperpolarizing responses immediately before the sound-evoked response for either response type (Fig. 3*G*), consistent with the absence of

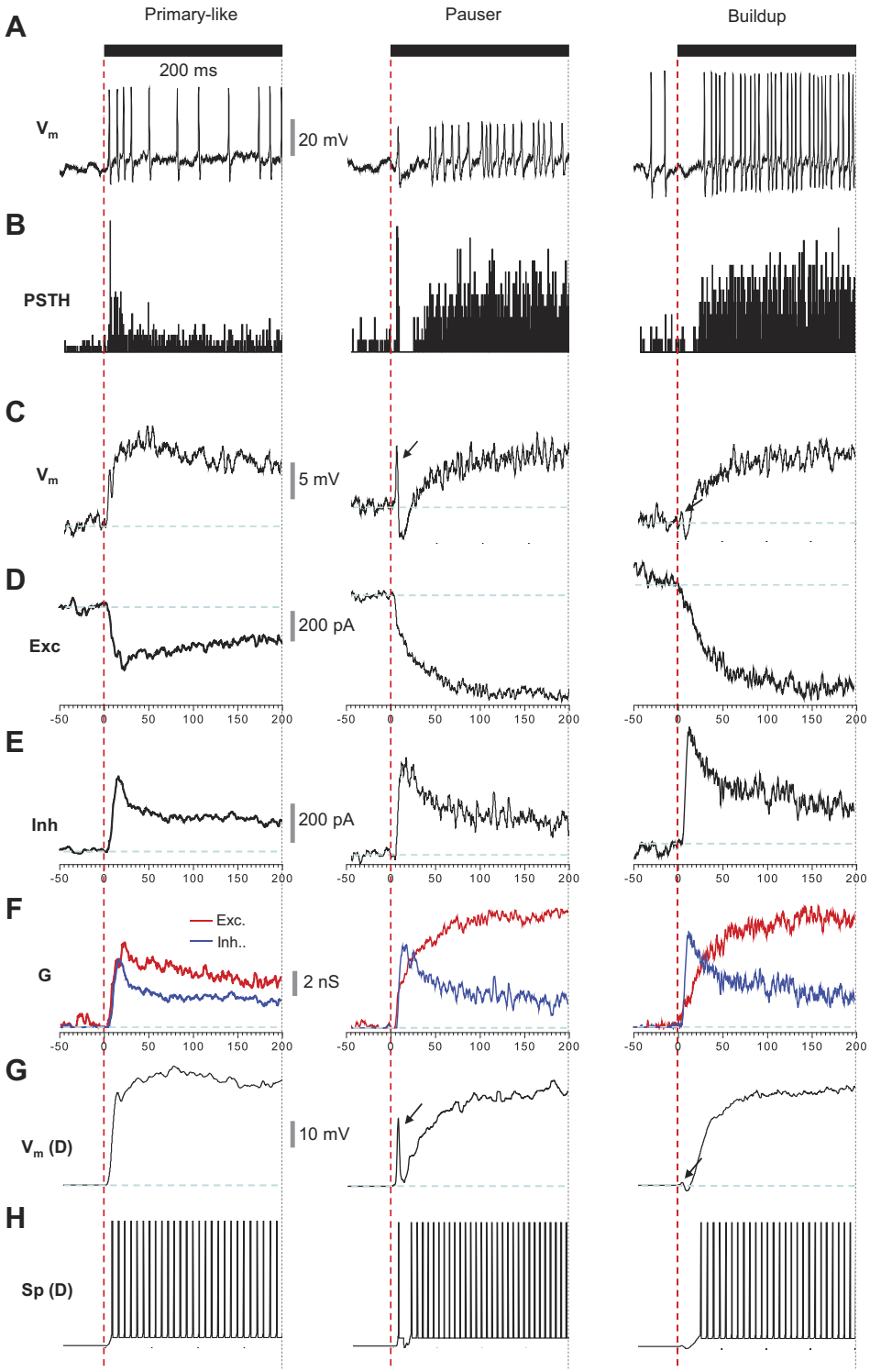

Fig. 2. Synaptic inputs underlying discharge patterns of 3 example pyramidal neurons. *A*: a raw trace of current-clamp recording (in 1 trial) in response to the CF tone (duration = 200 ms). Dashed, vertical lines mark the onset and offset of the tone stimulation. Scale bar is presented as a vertical bar (same as below). *B*: PSTH (bin size = 1 ms) for spikes recorded in all trials. *C*: average subthreshold membrane-potential (V_m) responses. Arrows indicate onset depolarizations. Blue, dashed lines represent baseline (same as below). *D*: average excitatory currents (Exc; 10 trials) recorded under voltage clamp. *E*: average inhibitory currents (Inh). *F*: superimposed-derived excitatory (red) and inhibitory (blue) synaptic conductances (G). Note that in primary-like, pauser, and buildup units, excitation onset precedes inhibition onset by 1.4 ms, 1.35 ms, and 0.6 ms, respectively. *G*: derived V_m [V_m (D)] responses by integrating the synaptic conductances shown in *F* with the neuron model. Arrows indicate onset depolarizations. *H*: derived spike responses [Sp (D)] after a 20-mV spike threshold (refractory period = 5 ms) was applied. Each vertical line represents a spike.

inhibitory input preceding the sound-evoked excitation (Fig. 3*F*). In addition, there was no significant difference in the membrane voltage immediately before the sound-evoked response among the three types of cells (Fig. 3*G*). Therefore, in the present study, it is difficult to explain the response diversity with a systematic variation in the prior membrane voltage among different cell classes.

We determined the quality of voltage-clamp recording by plotting the current-voltage (I–V) relationship for the recorded synaptic currents. As shown by an example cell (Fig. 3*H*), noise-evoked synaptic currents under four different holding potentials were averaged. The current amplitude at 4 ms after the response onset changed linearly with varying clamping voltages, with the derived reversal potential closely matching the expected reversal potential for excitatory currents (0 mV). The current amplitude at 16 ms after the response onset also changed linearly with the clamping voltage. However, the reversal potential for currents at this time point was approxi-

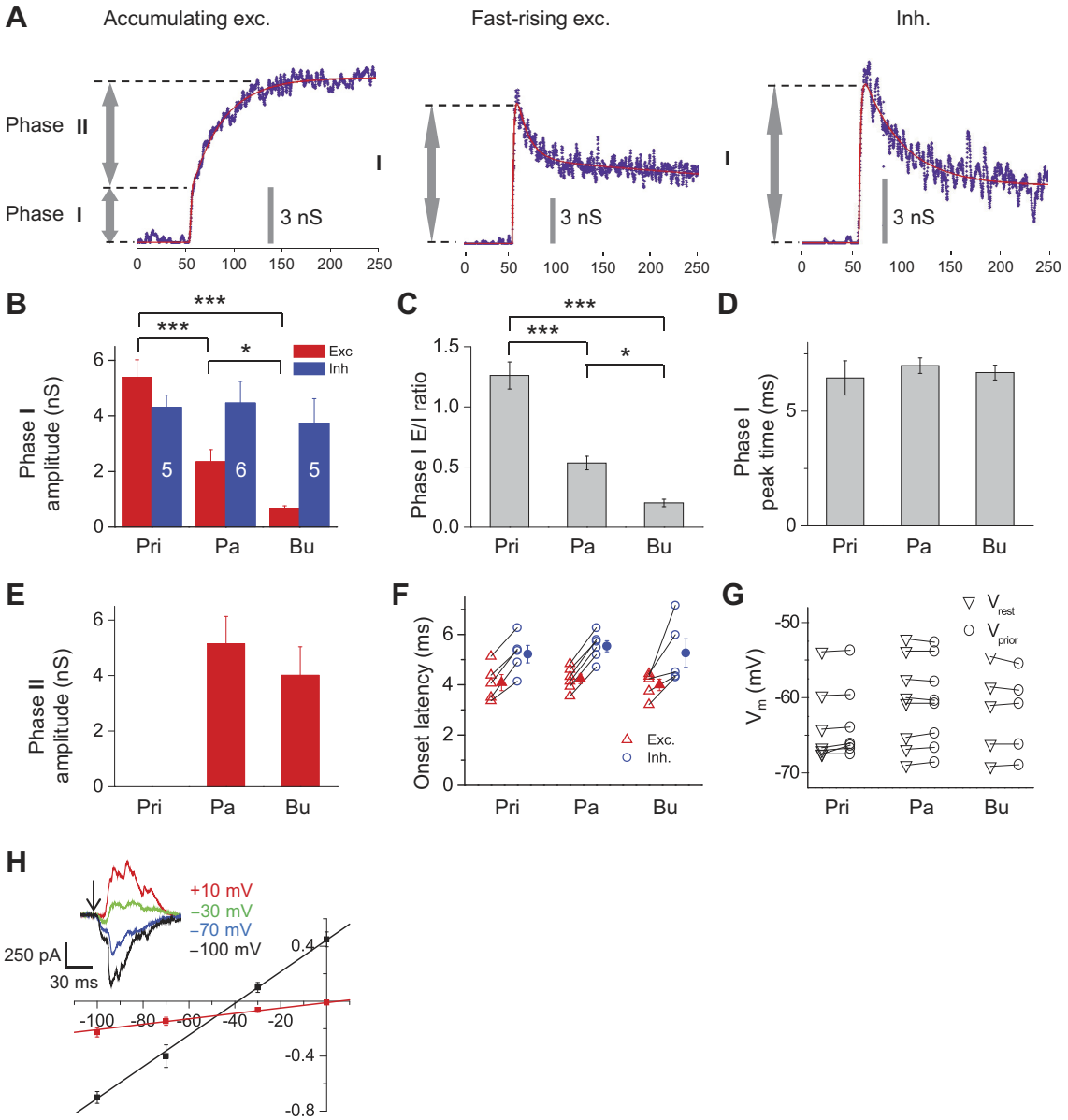

Fig. 3. Summary of properties of synaptic inputs to the 3 types of pyramidal neurons. *A*: example traces of accumulating excitation, fast-rising excitation, and inhibition. The best-fit curve for each trace is shown in red, and measurements of *phase I* and *phase II* amplitudes are illustrated with double arrowheads. *B*: average *phase I* amplitudes of excitation (red) and inhibition (blue) to 3 types of cells. Bars = SE; $***P < 0.001$, and $*P < 0.05$, 1-way ANOVA and post hoc Tukey test. Cell numbers are marked. *C*: average excitation/inhibition (E/I) ratios in *phase I*. *D*: average timing of the peak of *phase I* excitation relative to the tone onset. *E*: average amplitudes of *phase II* excitation. *F*: onset latencies of excitation and inhibition. Filled symbols indicate average values. *C–F*: cell numbers are the same as in *B*. *G*: resting V_m (V_{rest}; inverted triangle) and the average V_m within a 10-ms window right before the onset of tone-evoked responses (V_{prior}; circle). Data points for the same cell are connected with a line. No significant difference was found among groups (1-way ANOVA, $F = 1.80$, $P = 0.15$) or within groups ($P > 0.05$, paired *t*-test). *H*: current-voltage curve of recorded synaptic currents for an example cell in response to 60 dB noise. Current amplitudes at 4 ms (red symbol) and 16 ms (black symbol) after response onset were plotted against 4 different clamping voltage; $n = 10$. *Inset*: average synaptic currents trace under 4 different clamping voltage. Arrow indicates sound onset.

mately −39 mV, indicating a mixture of excitatory and inhibitory conductances. The linear I–V curves indicated that the quality of voltage clamp in our experimental conditions had been reasonably good.

Synaptic mechanisms for the generation of response diversity. To test further whether the differential temporal patterns of synaptic inputs, as we observed, can account for the diversity of spike response patterns, we carried out in vivo dynamic-clamp recordings (see MATERIALS AND METHODS) and revealed membrane-potential responses to injections of simulated excitatory and inhibitory conductances into the cell (Fig. 4*A*). Synaptic conductances were described by the arithmetic functions used for fitting experimental data (Fig. 4, *B* and *C*). To be consistent with experimental observations (Fig. 3, *B* and *E*), the amplitude and temporal profile of inhibitory conductance were fixed, whereas those of excitatory conductance were varied. To simulate pauser and buildup responses (Fig. 4*B*), the amplitude of *phase II* excitation was fixed, whereas that of *phase I* excitation was varied. Notably, a fast, transient depolarization was generated at the onset of the membrane-potential response, and its amplitude was dependent on the amplitude ratio between the *phase I* excitation and the inhibition (Fig. 4*B*). The larger the E/I ratio, the greater the amplitude of the

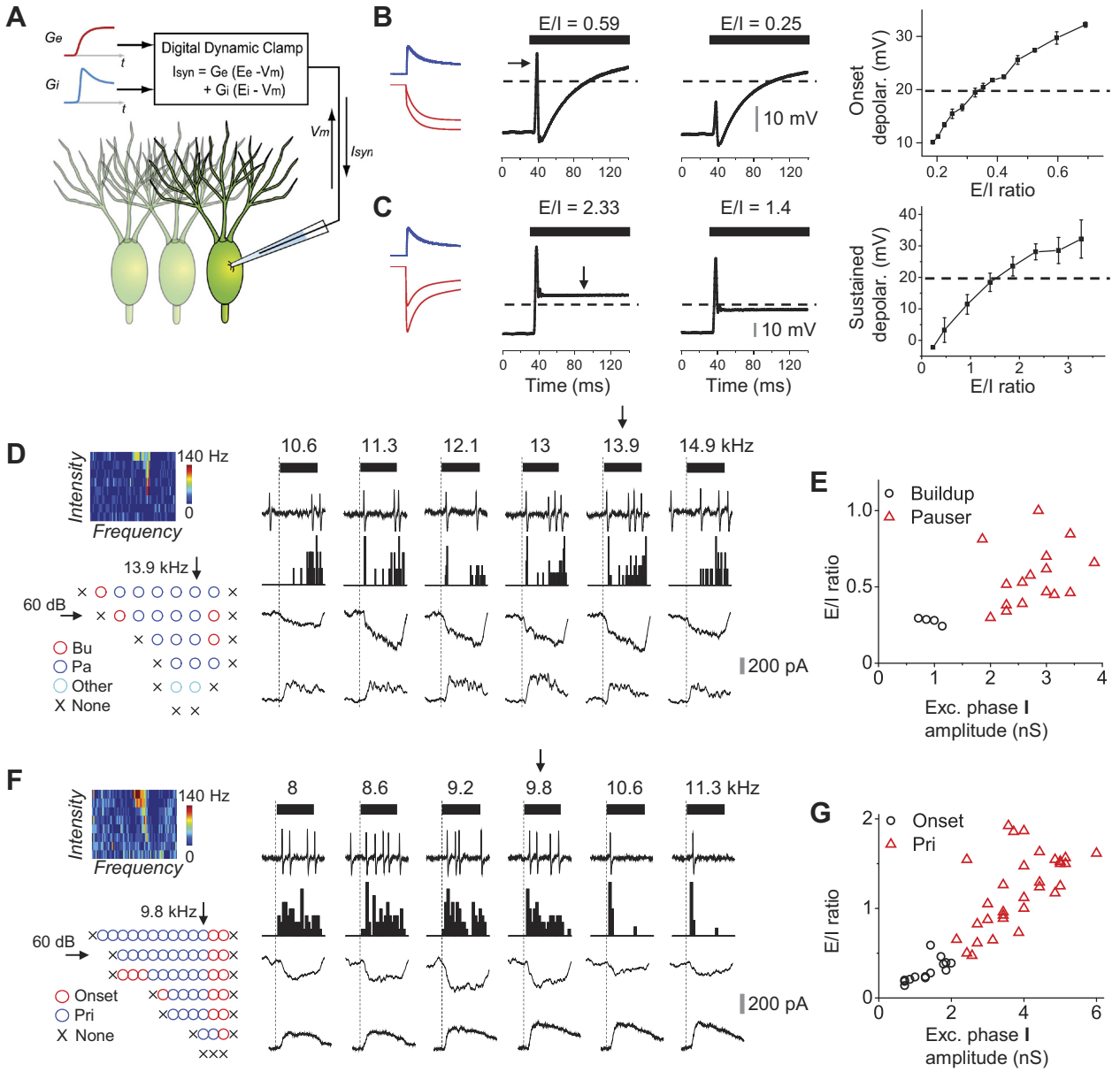

Fig. 4. A synaptic mechanism for the response diversity in the DCN. *A*: schematic illustration of dynamic-clamp recording. V_m is recorded from the patched cell. The synaptic current (I_{syn}) is calculated based on the V_m and modeled synaptic conductances and is injected into the cell in real time. G_e, excitatory synaptic conductance; G_i, inhibitory synaptic conductance; E_e, excitatory reversal potential; E_i, inhibitory reversal potential; *t*, time. *B, left*: temporal profiles of inhibition (blue) and accumulating excitation (red) simulated for pauser and buildup response patterns. The amplitude of *phase I* excitation was varied. *Middle*: V_m responses in the in vivo dynamic-clamp recording from a DCN pyramidal neuron. The E/I ratio between *phase I* excitation and inhibition is marked. Bars represent a 110-ms putative tone stimulus. Dash lines mark the putative spike threshold. *Right*: peak amplitude of the transient onset depolarization (marked by arrows in the *middle*), plotted against the E/I ratio between *phase I* excitation and inhibition. Bars = SE; $n = 4$ cells. *C, left* and *middle*: dynamic-clamp recording in the same cell as shown in *B* (*middle*). Fast-rising excitation with the peak amplitude varied was injected to simulate primary-like and onset cells. *Right*: amplitude of sustained depolarization (marked by arrows in the *middle*), plotted against the E/I ratio. Bars = SE; $n = 4$ cells. *D*, *left*: color map of the frequency-intensity tonal receptive field (TRF) of a pyramidal neuron (*top*) and the type of discharge pattern for tone-evoked responses within the TRF (*bottom*). Horizontal arrow points to the intensity level at 60 dB SPL. Vertical arrow points to the CF. "Other" is the delayed, sustained response pattern that resembles the primary-like pattern, except that the response onset delay was longer, and there was no apparent onset peak response; "None" is no significant tone-evoked response. *Right, top to bottom*: recorded trace of spike response, PSTH (bin size = 1 ms), and excitatory and inhibitory currents to effective tones at 60 dB SPL in the same cell. Vertical arrow points to the CF. *E*: plot of E/I ratio vs. amplitude of *phase I* excitation for all of the identified buildup and pauser responses within the TRF of the cell shown in *D*. *F*: TRF and response patterns for another example cell. *G*: plot of E/I ratio vs. amplitude of *phase I* excitation for all of the identified onset and primary-like responses within the TRF of the cell shown in *F*.

transient-onset depolarization (Fig. 4*B*). After a delay, the membrane voltage gradually increased to a level above the spike threshold (Fig. 4*B*). Therefore, the putative spike pattern would be of pauser or buildup type, depending on whether the transient-onset depolarization was large enough to cross the spike threshold. In the same recorded cell, the simulated excitation and inhibition of primary-like responses generated a large, fast transient depolarization, followed by a smaller, sustained depolarization (Fig. 4*C*). The amplitude of the sustained depolarization depended on the E/I ratio (Fig. 4*C*). Therefore, the putative spike

pattern would be the primary-like type, if the sustained depolarization were large and crossed the spike threshold, or of onset type, if it were below the spike threshold.

It was previously reported that the same DCN neuron could exhibit different discharge patterns in a stimulus-dependent manner under different tone frequencies and intensities (Hancock and Voigt 2002; Rhode et al. 1983). This could be potentially attributed to a similar synaptic mechanism, since the strengths of synaptic inputs and E/I ratio can be modulated by frequency and intensity. We thus examined the spike and synaptic responses to all effective tones within the TRF of individual cells. The example cell in Fig. 4*D* was identified as a pauser cell based on its spike response pattern to the CF tone (13.9 kHz) at a relatively high intensity (60 dB SPL). At this intensity level, whereas the cell exhibited pauser discharge patterns to 11.3, 12.1, 13, and 13.9 kHz tones, it displayed buildup-discharge patterns to 10.6 and 14.9 kHz tones (Fig. 4*D*). Such variation in discharge pattern was observed at other tone intensities as well (Fig. 4*D*). We plotted the synaptic parameters for the corresponding identified discharge patterns within the TRF (Fig. 4*E*). It became clear that buildup patterns were associated with small excitatory input amplitudes and small E/I ratios during *phase I*, whereas pauser patterns were associated with larger amplitudes of *phase I* excitation and larger E/I ratios. There was no difference in the membrane potential before the sensory-evoked response between the two groups of responses ($P > 0.05$, *t*-test). Another example cell (Fig. 4*F*) was identified as a primary-like type, based on its spike response pattern to the CF tone (9.8 kHz) at 60 dB SPL. However, its discharge patterns to frequencies above the CF were clearly of onset type, consisting only of a transient onset response (Fig. 4*F*). For all of the tone-evoked responses, onset patterns were associated with smaller *phase I* excitation and smaller E/I ratios compared with primary-like patterns. Again, there was no difference in the membrane potential before the sensory-evoked response between the two groups of responses ($P > 0.05$, *t*-test). Together, these experimental observations validate the predictions from the dynamic-clamp experiment that differential excitatory temporal profiles can well separate the primary-like/onset types from pauser/buildup types and that the strength of excitation and the E/I ratio during *phase I* can further distinguish pauser from buildup responses or primary-like from onset responses.

Potential excitatory input sources for pyramidal neurons. That the excitatory input may contain two distinct components of fast- and slow-rising kinetics is reminiscent of previous findings that DCN pyramidal neurons primarily receive excitatory inputs from two sources: the auditory nerve input onto their basal dendrites and the parallel fiber input onto their apical dendrites (Fig. 5*A*). Zhang and Oertel (1994) showed that DCN pyramidal cells can respond to electrical stimulation of the auditory nerve with a slowly rising excitatory postsynaptic potential, which remains after severing the branches of auditory nerve fibers directly innervating the pyramidal cells. Kuo and Trussell (2011) showed that parallel fibers exhibit strong short-term facilitation. These results together suggest that the parallel fiber input is delayed relative to the direct auditory nerve input and that the second excitatory component that we observed in vivo might be contributed by parallel fiber inputs. Whereas it is difficult to separate excitatory inputs of

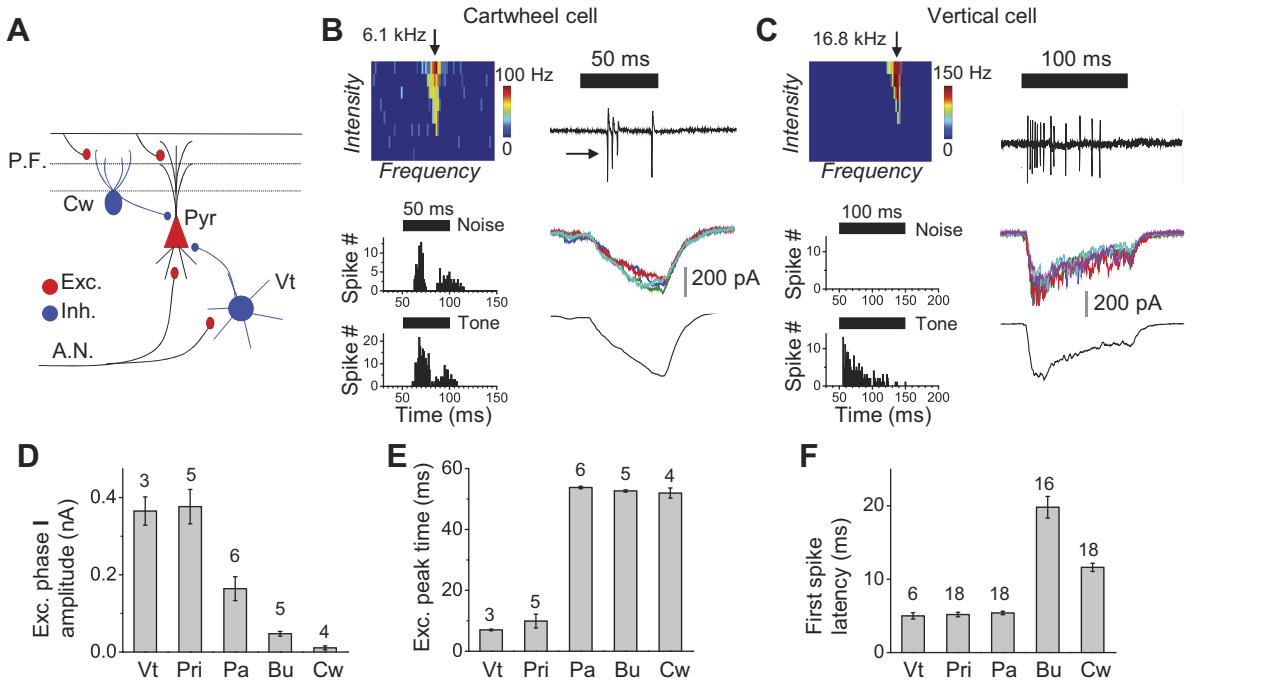

Fig. 5. Potential circuit mechanisms for generating response diversity in the DCN. *A*: schematic drawing of DCN circuits. A.N., auditory nerve; P.F., parallel fiber; Vt, vertical cell; Cw, cartwheel cell; Pyr, pyramidal cell. Red and blue dots represent excitatory and inhibitory synapses, respectively. *B, left*: color map of the TRF (*top*) of an example cartwheel cell and the PSTHs for responses to noise and CF tone stimuli (marked by the bars). Vertical arrow points to the CF. *Right*: cell-attached recording of spike responses (*top*), superimposed excitatory currents of 4 trials (*middle*), and average excitatory current (*bottom*). Arrow points to the complex spike. Tone duration is marked by the bar. *C*: TRF and responses to noise and CF tone stimuli of a vertical cell. Note that it exhibited 0 spontaneous firing rate and no response to noise stimulation. *Right*: evoked spikes and excitatory currents by CF tones. *D*: average amplitude of *phase I* excitation for different types of cells. Bars = SE; cell numbers are marked. *E*: average timing of peak excitatory amplitude relative to the tone onset. Cell numbers are the same as in *D*. *F*: average 1st spike latency. Cell numbers are marked.

the two different sources in vivo, we may be able to estimate their temporal properties by examining the sound-evoked excitatory inputs to cartwheel and vertical cells, respectively. Previous studies suggest that vertical cells are driven primarily by auditory nerve inputs (Spirou et al. 1999), whereas cartwheel cells predominantly receive excitation from parallel fibers (Fujino and Oertel 2003) (Fig. 5*A*). Therefore, the temporal properties of excitation to cartwheel and vertical cells may reflect that of parallel fiber and auditory nerve inputs, respectively.

In our recordings, cartwheel cells were identified by the firing of complex spikes (Fig. 5*B*), according to previous studies (Manis et al. 1994; Parham and Kim 1995; Portfors and Roberts 2007). Vertical cells were identified by the extremely low, spontaneous firing rates (<0.05 spikes/s) and the lack of responses to noise stimuli (Rhode 1999; Spirou et al. 1999; Young and Brownell 1976) (Fig. 5*C*). Subsequent voltage-clamp recordings from the same cells then revealed their tone-evoked excitation (Fig. 5, *B* and *C*). With similar curve-fitting methods, as shown in Fig. 3*A*, we quantified the amplitudes and temporal profiles of the excitatory currents in vertical and cartwheel cells. Notably, the excitation in vertical cells was similar to that in primary-like pyramidal cells, since they both exhibited a large amplitude of *phase I* excitation (Fig. 5*D*) and a very short delay to the maximum excitatory response (i.e., fast rising; Fig. 5*E*). These results support the notion that the fast-rising excitation in primary-like neurons could be attributed mainly to the auditory nerve input, which drives rapid spiking of these and vertical cells with similar latencies (Fig. 5*F*). On the other hand, the slowly accumulating excitation in cartwheel cells resembled the *phase II* excitation in pauser and buildup neurons, as demonstrated by the long delay to the maximum amplitude (Fig. 5*E*). This result suggests that parallel fiber inputs likely assume a slowly accumulating property and contribute largely to the *phase II* excitation in pauser and buildup neurons. We also noticed that the *phase I* excitation in pauser and buildup neurons resembled the fast-rising excitation in primary-like neurons in terms of onset latency (Fig. 3*F*) and rising speed (pauser, $\tau = 7.08 \pm 0.99$ ms, mean ± SD; buildup, $\tau = 7.64 \pm 2.57$ ms; primary-like, $\tau = 5.19 \pm 1.26$ ms; one-way ANOVA, $F = 1.62$, $P = 0.27$). This suggests that the *phase I* excitation may be attributed to direct auditory nerve inputs.

DISCUSSION

In this study, we applied in vivo whole-cell recordings to examine the possible synaptic mechanisms underlying differential temporal response patterns in the DCN. We found that the differences in discharge pattern were sufficiently attributable to differential temporal profiles and amplitudes of excitatory synaptic inputs received by DCN pyramidal neurons. Those receiving dominant fast-rising excitation exhibit primary-like or onset responses, depending on the E/I ratio in the initial response rising phase. Neurons receiving accumulating excitation exhibit pauser or buildup responses, again, depending on the E/I ratio in the initial fast response rising phase.

Potential sources of excitatory inputs. The differential excitatory temporal profiles may be due to variations in how DCN pyramidal cells sample from two potential excitatory input sources. For primary-like cells, their inputs can be primarily from auditory nerve fibers, since the temporal profile of these inputs closely resembles that of auditory nerve firing (Kiang et al. 1965). For pauser and buildup cells, their inputs are likely a mixture, from both auditory nerve and parallel fibers. The auditory nerve input to pauser cells is probably strong enough to trigger a fast-onset spike response, as the first spike latency of these cells is similar to that of primary-like and vertical cells. The auditory nerve input to buildup cells is relatively weak, and their spiking has to rely on the second-phase excitation to accumulate to a certain level to overcome inhibition, resulting in a much longer delay for the first spike to appear. These results suggest that the differential excitatory input patterns plus corresponding physiological ranges of amplitude would directly lead to distinct temporal patterns of membrane-potential responses, with the distinction depending on whether a fast onset spike response can be generated and whether there is a following suppression period. The functional type of the cells was defined based on their responses to CF tones at a relatively high intensity. For an individual cell, the excitatory input pattern as well as the E/I ratio can vary depending on the tone frequency and intensity, resulting in a stimulus-dependent variation in discharge pattern.

We propose that the slow-rising excitatory inputs to buildup and pauser cells can be from parallel fibers projected by granule cells. This is mostly based on the observation that cartwheel cells, which receive parallel fiber inputs, exhibit slow-rising excitation. However, the nature of auditory information carried by parallel fibers remains unknown, except for the anatomical evidence that granule cells in the cochlear nucleus receive inputs from both *type II* auditory nerve (Brown et al. 1988; Brown and Ledwith 1990) and efferent auditory (Kane and Finn 1977) fibers. Additionally, it has been suggested that nonauditory information relayed by parallel fibers can modulate the spike rate and spike timing of fusiform cells (Kanold et al. 2011; Koehler et al. 2011; Koehler and Shore 2013; Oertel and Young 2004). An alternative hypothesis would be that both fusiform cells and cartwheel cells receive slow-rising excitation from another excitatory source. For example, T-type multipolar cells in the posterior ventral cochlear nucleus, which project to the DCN (Oertel et al. 1990; Smith and Rhode 1989), may contribute to the excitation in fusiform cells. The sources of excitation to fusiform cells need to be investigated further in the future with anatomical and functional synaptic-connection studies.

Potential sources of inhibitory inputs. Our data indicate that the three cell types receive inhibitory inputs with similar temporal patterns in response to 60 dB CF tones. Previous studies have proposed that fusiform cells receive both central-area inhibition from vertical cells and wide-band inhibition from putative D-type multipolar cells (Nelken and Young 1994). In addition, fusiform cells receive inhibitory inputs from cartwheel cells. The temporal firing patterns of vertical and D-type multipolar cells have been shown to be of primary-like type, onset, and onset chopper types (Rhode 1999; Smith and Rhode 1989), whereas the sound-evoked discharge of cartwheel cells exhibits a longer onset delay (Fig. 5*F*) with complex spike patterns (Fig. 5*B*). Based on these output firing patterns, it is possible that a mixture of inhibitory inputs from these neurons together can construct a temporal profile similar to what has been observed in fusiform cells. We should note that despite the similarities of inhibitory patterns, it is the interplay of excita-

tion and inhibition within appropriate ranges of amplitude that eventually generates the different response types. For example, it is likely that removal of inhibition to pauser cells can convert their responses to a sustained type.

Synaptic vs. intrinsic mechanisms. Intrinsic conductances of fusiform cells have been shown previously to affect their firing patterns (Kanold and Manis 1999, 2005; Leao et al. 2012; Manis 1990). Manis and colleagues (Kanold and Manis 1999, 2005; Manis 1990) demonstrated in slice recordings that three distinct temporal discharge patterns of DCN pyramidal neurons could be elicited by current injections, depending on the level of the holding potential before the depolarization induced by the injected current. Buildup and pauser responses were observed if the cells were held hyperpolarized before the induced depolarization. In this study, our current-clamp recordings in vivo did not reveal significant differences in the membrane potential preceding the sound-evoked responses among different types of neurons or among different types of responses in an individual neuron. Instead, our results suggest an important contribution from the heterogeneity of synaptic inputs to the diversity of discharge patterns. In particular, our dynamic-clamp recordings demonstrate that synaptic inputs with physiologically relevant temporal profiles and amplitudes can be sufficient for generating diverse temporal response patterns. It should be noted that these results were obtained in anesthetized conditions, which affect intrinsic conductances, and under relatively simple acoustic stimulation paradigms. They do not exclude any potential contribution of an intrinsic membrane-conductance mechanism to the response diversity, since intrinsic conductances plus prior history activity are also shown to be sufficient for generating diverse discharge patterns. It is possible that in awake conditions or under more complicated stimulation paradigms (e.g., naturalistic sounds), synaptic mechanisms and intrinsic membrane-conductance mechanisms work synergistically to influence spike response patterns. This remained to be investigated further in future studies.

Technical considerations. To reveal the synaptic inputs and membrane-potential outputs of the same neuron, we performed whole-cell voltage-clamp and current-clamp recordings in the same cell. Several lines of evidence suggested that the DCN neurons in our experiments were clamped at desired potentials. First, the linear I–V curve (Fig. 3*H*) suggested that voltage-dependent conductances contributed little to the recorded currents under our experimental conditions. Second, the I–V curve (Fig. 3*H*) for the evoked currents within a 4-ms window from the response onset (excitatory in nature) roughly crossed the origin (0, 0), indicating that the measured reversal potential indeed closely matched the expected reversal potential of excitatory currents (0 mV). In other words, the intended clamping voltage of 0 mV was achieved with reasonable precision. Third, although the reversal potentials were already determined by the intracellular and extracellular ionic concentrations, we arbitrarily set the reversal potential for inhibitory currents at -60 or -80 mV (i.e., ± 10 mV shift from the expected reversal potential) and found that this did not change the conclusion of this study. The derived synaptic conductances could still generate the three different temporal discharge patterns. Finally, in our neuron modeling, the membrane-potential response patterns derived from the observed excitatory and inhibitory inputs qualitatively matched those recorded under current clamp in the same cell (Fig. 2, *C* and *G*), suggesting that the measured synaptic conductances could largely account for the observed membrane-potential response. Together, these results demonstrate that the recorded currents well reflect the underlying synaptic inputs. Nevertheless, it should be noted that the cable effect and potential space-clamp errors would affect the recorded amplitudes of synaptic inputs, with less deleterious effects on their temporal dynamics (Tan et al. 2004). How active dendritic conductances contribute to the auditory processing in DCN neurons needs to be investigated in future studies.

Functional implications. DCN neurons were categorized based on either receptive field structures (Evans and Nelson 1973) or temporal discharge patterns to CF tones (Godfrey et al. 1975). Based on receptive field properties of its neurons, the DCN has been proposed to use spectral cues to localize sound in the vertical plane (Bandyopadhyay and Young 2013; Nelken and Young 1994; Oertel and Young 2004). The functional significance of temporal discharge patterns is less clear. We speculate that with the diverse responses in a transient time window (~25 ms) after sound onsets, the DCN can play a role in diverse coding of sound onset information. This likely forms a foundation for the parallel processing of acoustic information in higher-level auditory centers. DCN response properties are strongly influenced by inhibition (Nelken and Young 1994; Oertel and Young 2004; Zhou et al. 2012), which may endow this processing center with an advantage in generating novel response properties that allow detection of important features in the acoustic environment. Whereas our current study provides a plausible synaptic circuitry mechanism for the generation of diverse temporal response patterns in DCN pyramidal cells, it should be noted that it remains a great challenge to resolve the circuitry underlying various specific processing functions. Future studies with genetic/optogenetic tools will be needed to dissect the role of each different type of neuron in the functional circuitry of the DCN.

GRANTS

Support for this work was provided to L. I. Zhang by grants from the National Institute on Deafness and Other Communication Disorders (R01DC008983) and the David and Lucile Packard Foundation (Packard Fellowships for Science and Engineering). H. W. Tao was supported by a grant from the National Eye Institute (R01EY019049). W. Yuan was supported by grants from the National Natural Science Foundation of China (NSFC; 30973301, 81271080, and 81470694).

DISCLOSURES

No conflicts of interest, financial or otherwise, are declared by the authors.

AUTHOR CONTRIBUTIONS

Author contributions: H.W.T. and L.I.Z. conception and design of research; M.Z. and Y-T.L. performed experiments; M.Z., H.W.T., and L.I.Z. analyzed data; M.Z., W.Y., H.W.T., and L.I.Z. interpreted results of experiments; M.Z. prepared figures; M.Z. drafted manuscript; H.W.T. and L.I.Z. edited and revised manuscript; M.Z., Y-T.L., W.Y., H.W.T., and L.I.Z. approved final version of manuscript.

REFERENCES

Bandyopadhyay S, Young ED. Nonlinear temporal receptive fields of neurons in the dorsal cochlear nucleus. *J Neurophysiol* 110: 2414–2425, 2013.

Brown MC, Berglund AM, Kiang NY, Ryugo DK. Central trajectories of type II spiral ganglion neurons. *J Comp Neurol* 278: 581–590, 1988.

Brown MC, Ledwith JV III. Projections of thin (type-II) and thick (type-I) auditory-nerve fibers into the cochlear nucleus of the mouse. *Hear Res* 49: 105–118, 1990.

Chung S, Ferster D. Strength and orientation tuning of the thalamic input to simple cells revealed by electrically evoked cortical suppression. *Neuron* 20: 1177–1189, 1998.

Ehret G, Merzenich MM. Complex sound analysis (frequency resolution, filtering and spectral integration) by single units of the inferior colliculus of the cat. *Brain Res* 472: 139–163, 1988.

Evans E, Nelson P. The responses of single neurones in the cochlear nucleus of the cat as a function of their location and the anaesthetic state. *Exp Brain Res* 17: 402–427, 1973.

Fujino K, Oertel D. Bidirectional synaptic plasticity in the cerebellum-like mammalian dorsal cochlear nucleus. *Proc Natl Acad Sci USA* 100: 265–270, 2003.

Godfrey DA, Kiang NY, Norris BE. Single unit activity in the dorsal cochlear nucleus of the cat. *J Comp Neurol* 162: 269–284, 1975.

Golding NL, Oertel D. Physiological identification of the targets of cartwheel cells in the dorsal cochlear nucleus. *J Neurophysiol* 78: 248–260, 1997.

Hancock KE, Voigt HF. Intracellularly labeled fusiform cells in dorsal cochlear nucleus of the gerbil. I. Physiological response properties. *J Neurophysiol* 87: 2505–2519, 2002.

Hines M. NEURON—a program for simulation of nerve equations. In: *Neural Systems: Analysis and Modeling*, edited by Eeckman F. Norwell, MA: Kluwer, 1993, p. 127–136.

Jagadeesh B, Wheat HS, Kontsevich LL, Tyler CW, Ferster D. Direction selectivity of synaptic potentials in simple cells of the cat visual cortex. *J Neurophysiol* 78: 2772–2789, 1997.

Kane ES, Finn R. Desending and intrinsic inputs to dorsal cochlear nucleus of cats: a horseradish peroxidase study. *Neuroscience* 2: 897–912, 1977.

Kanold PO, Davis KA, Young ED. Somatosensory context alters auditory responses in the cochlear nucleus. *J Neurophysiol* 105: 1063–1070, 2011.

Kanold PO, Manis PB. Encoding the timing of inhibitory inputs. *J Neurophysiol* 93: 2887–2897, 2005.

Kanold PO, Manis PB. Transient potassium currents regulate the discharge patterns of dorsal cochlear nucleus pyramidal cells. *J Neurosci* 19: 2195–2208, 1999.

Kiang NY, Watanabe T, Thomas EC, Clark LF. *Discharge Patterns of Single Fibers in the Cat's Auditory Nerve*. Cambridge, MA: MIT Press, 1965.

Koehler SD, Pradhan S, Manis PB, Shore SE. Somatosensory inputs modify auditory spike timing in dorsal cochlear nucleus principal cells. *Eur J Neurosci* 33: 409–420, 2011.

Koehler SD, Shore SE. Stimulus-timing dependent multisensory plasticity in the guinea pig dorsal cochlear nucleus. *PLoS One* 8: e59828, 2013.

Kuo SP, Lu HW, Trussell LO. Intrinsic and synaptic properties of vertical cells of the mouse dorsal cochlear nucleus. *J Neurophysiol* 108: 1186–1198, 2012.

Kuo SP, Trussell LO. Spontaneous spiking and synaptic depression underlie noradrenergic control of feed-forward inhibition. *Neuron* 71: 306–318, 2011.

Kuwada S, Batra R, Yin TC, Oliver DL, Haberly LB, Stanford TR. Intracellular recordings in response to monaural and binaural stimulation of neurons in the inferior colliculus of the cat. *J Neurosci* 17: 7565–7581, 1997.

Leao RM, Li S, Doiron B, Tzounopoulos T. Diverse levels of an inwardly rectifying potassium conductance generate heterogeneous neuronal behavior in a population of dorsal cochlear nucleus pyramidal neurons. *J Neurophysiol* 107: 3008–3019, 2012.

Li YT, Ma WP, Pan CJ, Zhang LI, Tao HW. Broadening of cortical inhibition mediates developmental sharpening of orientation selectivity. *J Neurosci* 32: 3981–3991, 2012.

Liu BH, Li YT, Ma WP, Pan CJ, Zhang LI, Tao HW. Broad inhibition sharpens orientation selectivity by expanding input dynamic range in mouse simple cells. *Neuron* 71: 542–554, 2011.

Liu BH, Wu GK, Arbuckle R, Tao HW, Zhang LI. Defining cortical frequency tuning with recurrent excitatory circuitry. *Nat Neurosci* 10: 1594–1600, 2007.

Manis PB. Membrane properties and discharge characteristics of guinea pig dorsal cochlear nucleus neurons studied in vitro. *J Neurosci* 10: 2338–2351, 1990.

Manis PB, Spirou GA, Wright DD, Paydar S, Ryugo DK. Physiology and morphology of complex spiking neurons in the guinea pig dorsal cochlear nucleus. *J Comp Neurol* 348: 261–276, 1994.

Mugnaini E, Warr WB, Osen KK. Distribution and light microscopic features of granule cells in the cochlear nuclei of cat, rat, and mouse. *J Comp Neurol* 191: 581–606, 1980.

Nelken I, Young ED. Two separate inhibitory mechanisms shape the responses of dorsal cochlear nucleus type IV units to narrowband and wideband stimuli. *J Neurophysiol* 71: 2446–2462, 1994.

Oertel D, Wu SH, Garb MW, Dizack C. Morphology and physiology of cells in slice preparations of the posteroventral cochlear nucleus of mice. *J Comp Neurol* 295: 136–154, 1990.

Oertel D, Young ED. What's a cerebellar circuit doing in the auditory system? *Trends Neurosci* 27: 104–110, 2004.

Parham K, Kim DO. Spontaneous and sound-evoked discharge characteristics of complex-spiking neurons in the dorsal cochlear nucleus of the unanesthetized decerebrate cat. *J Neurophysiol* 73: 550–561, 1995.

Portfors CV, Roberts PD. Temporal and frequency characteristics of cartwheel cells in the dorsal cochlear nucleus of the awake mouse. *J Neurophysiol* 98: 744–756, 2007.

Recanzone GH. Response profiles of auditory cortical neurons to tones and noise in behaving macaque monkeys. *Hear Res* 150: 104–118, 2000.

Rhode WS. Vertical cell responses to sound in cat dorsal cochlear nucleus. *J Neurophysiol* 82: 1019–1032, 1999.

Rhode WS, Kettner RE. Physiological study of neurons in the dorsal and posteroventral cochlear nucleus of the unanesthetized cat. *J Neurophysiol* 57: 414–442, 1987.

Rhode WS, Smith PH. Physiological studies on neurons in the dorsal cochlear nucleus of cat. *J Neurophysiol* 56: 287–307, 1986.

Rhode WS, Smith PH, Oertel D. Physiological response properties of cells labeled intracellularly with horseradish peroxidase in cat dorsal cochlear nucleus. *J Comp Neurol* 213: 426–447, 1983.

Ryugo DK, May SK. The projections of intracellularly labeled auditory nerve fibers to the dorsal cochlear nucleus of cats. *J Comp Neurol* 329: 20–35, 1993.

Semple MN, Kitzes LM. Single-unit responses in the inferior colliculus: different consequences of contralateral and ipsilateral auditory stimulation. *J Neurophysiol* 53: 1467–1482, 1985.

Smith PH, Rhode WS. Structural and functional properties distinguish two types of multipolar cells in the ventral cochlear nucleus. *J Comp Neurol* 282: 595–616, 1989.

Somers DC, Nelson SB, Sur M. An emergent model of orientation selectivity in cat visual cortical simple cells. *J Neurosci* 15: 5448–5465, 1995.

Spirou GA, Davis KA, Nelken I, Young ED. Spectral integration by type II interneurons in dorsal cochlear nucleus. *J Neurophysiol* 82: 648–663, 1999.

Stuart G, Spruston N. Determinants of voltage attenuation in neocortical pyramidal neuron dendrites. *J Neurosci* 18: 3501–3510, 1998.

Sun YJ, Wu GK, Liu BH, Li P, Zhou M, Xiao Z, Tao HW, Zhang LI. Fine-tuning of pre-balanced excitation and inhibition during auditory cortical development. *Nature* 465: 927–931, 2010.

Tan AY, Zhang LI, Merzenich MM, Schreiner CE. Tone-evoked excitatory and inhibitory synaptic conductances of primary auditory cortex neurons. *J Neurophysiol* 92: 630–643, 2004.

Wouterlood FG, Mugnaini E. Cartwheel neurons of the dorsal cochlear nucleus: a Golgi-electron microscopic study in rat. *J Comp Neurol* 227: 136–157, 1984.

Wu GK, Arbuckle R, Liu BH, Tao HW, Zhang LI. Lateral sharpening of cortical frequency tuning by approximately balanced inhibition. *Neuron* 58: 132–143, 2008.

Young ED, Brownell WE. Responses to tones and noise of single cells in dorsal cochlear nucleus of unanesthetized cats. *J Neurophysiol* 39: 282–300, 1976.

Zhang LI, Tan AY, Schreiner CE, Merzenich MM. Topography and synaptic shaping of direction selectivity in primary auditory cortex. *Nature* 424: 201–205, 2003.

Zhang M, Liu Y, Wang SZ, Zhong W, Liu BH, Tao HW. Functional elimination of excitatory feedforward inputs underlies developmental refinement of visual receptive fields in zebrafish. *J Neurosci* 31: 5460–5469, 2011.

Zhang S, Oertel D. Neuronal circuits associated with the output of the dorsal cochlear nucleus through fusiform cells. *J Neurophysiol* 71: 914–930, 1994.

Zhou M, Tao HW, Zhang LI. Generation of intensity selectivity by differential synaptic tuning: fast-saturating excitation but slow-saturating inhibition. *J Neurosci* 32: 18068–18078, 2012.